第 43 卷 第 17 期/2023 年 9 月/光学学报 特邀综述

光学学报

空间调制型偏振检测技术研究现状及发展趋势

高超[1,2]，翁剑宇[1,2]，曹晓昱[1,2]，张斌[1,2]，雷兵[1,2*]

[1]国防科技大学前沿交叉学科学院，湖南 长沙 410073；

[2]国防科技大学南湖之光实验室，湖南 长沙 410073

摘要 空间调制型偏振检测技术是利用微偏振片阵列、角向或径向偏振片、涡旋波片等器件对光强分布进行空间调制以实现偏振信息测量的一种技术，具有光路结构简单、稳定性好、测量速度快、精度高等优势，在目标探测识别、工业及生化检测等领域具有重要应用。首先，对各种空间调制型Stokes矢量和Mueller矩阵偏振检测技术的工作原理、技术特点进行综述分析；然后，对近年来发展迅速的基于涡旋波片的空间调制型偏振检测技术进行详细阐述，重点对基于涡旋半波片和1/4波片的Stokes偏振仪、基于双涡旋波片的Mueller矩阵偏振仪的工作原理、检测效果和误差校准等内容进行介绍；最后，对空间调制型偏振检测技术的主要发展趋势进行展望。

关键词 偏振检测；空间调制；Stokes矢量；Mueller矩阵；涡旋波片

中图分类号 O436 **文献标志码** A **DOI**：10.3788/AOS230925

1 引 言

偏振是光波的基本属性之一，也是重要的信息载体。任何目标在发射或反射（散射、透射、衍射）光波的过程中都会表现出由其自身特性和光学基本定理所决定的偏振特性[1]，通过对光波偏振特性进行检测分析，可以获得目标材质、复折射率、反射率、表面法线方向等信息，而这类信息是单纯利用传统的光强探测技术难以得到的[2]。偏振检测是在传统光强探测的基础上，进一步获得待测光波的偏振信息（偏振度、偏振方向、偏振旋向及偏振椭圆度等），并结合光与物质相互作用机理，反演出待测样品信息的一种光学检测技术。偏振检测充分利用了光波的偏振特征信息，能够显著提高对目标信息的获取分析能力。目前，偏振检测技术已在遥感探测[3-5]、薄膜参数测量[6-7]、工业检测[8-9]、集成电路[10-11]、光伏太阳能[12-13]、食品加工[14]、农业生产[15-16]、生物医学[17-20]、环境与海洋监测[21-23]、光通信[24-26]、仿生导航[27]和天文观测[28-29]等领域得到了广泛的应用。

Stokes（斯托克斯）矢量能够完全描述光波的任何偏振状态，4×4阶的Mueller（穆勒）矩阵能够完全描述物质与偏振光相互作用时所呈现的光学特性。因此，偏振检测技术的关键是获取待测光波的Stokes矢量或待测样品的Mueller矩阵，它们分别对应Stokes偏振检测技术与Mueller矩阵偏振检测技术，相应的检测仪器被称为Stokes偏振仪与Mueller矩阵偏振仪[30-31]。由于Stokes矢量有4个自由度，因此需要获取至少4种独立偏振调制状态下的光强信息才能解算出Stokes矢量的全部分量，即实现光波的全偏振检测。样品Mueller矩阵的测量则需要Mueller矩阵偏振仪的起偏臂与检偏臂相互配合完成，Mueller矩阵偏振仪的检偏臂通常采用与Stokes偏振仪相似的配置，起偏臂中偏振光学元件的组成一般与检偏臂相同但排列顺序相反[32]，测量时起偏臂产生至少4种独立偏振状态的光波入射至待测样品，检偏臂则对每一状态出射光的偏振态进行测量。因此，要获得全部的Mueller矩阵元素，需要测量得到起偏臂与检偏臂设置在至少16种不同状态下的光强值[30,33]。

目前，已有多种实现Stokes矢量、Mueller矩阵偏振检测的方法，根据测量原理可分为分光型和调制型两大类。分光型偏振检测是利用分光器件或子系统构建多个测量通道，通过在各通道中设置不同的偏振光学元件和探测器来同时获取不同状态下的输出光强，进而计算得到光波的Stokes矢量，具体有分波前和分振幅等形式[34-37]。分光型偏振仪可实时获得光波的不同偏振分量，数据处理简单，但多通道结构会增大设备体积、降低能量利用率，且多探测器的使用不仅会增加成本，也对其空间配准提出了严苛的要求。调制型偏振检测是在时间、空间和波长中的一个或多个域对待测光波的偏振信息进行调制和测量，分别对应时序调

收稿日期：2023-05-04；**修回日期**：2023-06-12；**录用日期**：2023-06-15；**网络首发日期**：2023-08-10

基金项目：国家自然科学基金（61975235）、湖南省自然科学基金（2019JJ40342）

通信作者：*leibing_2000@nudt.edu.cn

制、空间调制、波长调制和复合调制等方式[38-41]。调制型偏振检测虽然会使测量结果损失对应调制域的分辨率，但通过单个探测器便可实现偏振信息的测量，具有光路结构简单、成本较低的优势，是目前研究最多、应用最广的偏振检测技术。

时序调制型偏振检测系统通过旋转光路中的光学元件（偏振片、波片等）[42-44]或在光路中引入有源调制器件（电光、磁光、弹光、液晶等器件）[45-51]对光波的偏振态进行时序调制，并对调制后的光强进行测量分析，从而完成偏振检测。这类系统结构简单、数据处理方便、成本较低，但由于采用分时探测方式，实时性较差，且旋转光学元件存在的非共轴误差降低了系统的稳定性和精度。波长调制型偏振检测系统利用特定厚度比的多级波片将待测样品的Stokes-Mueller光谱信息调制到多个高频载波上，通过对光谱分析处理得到光波偏振态或样品的信息[52-53]。波长调制型偏振检测仪具有测量速度快、结构简单、无运动器件干扰等优点，但多级波片对光波的入射角度及环境温度较敏感，且多重信息复用给Stokes-Mueller光谱重构带来了巨大挑战，目前还缺乏简单高效的重构与标定方法。空间调制型偏振系统利用空间调制型器件对光波的偏振态进行调制，使其产生空间变化的光强分布，通过对光强调制图像进行分析处理便可得到偏振信息[54-58]。空间调制型偏振检测仪无需机械运动或有源器件，光路结构简单、稳定性好、测量速度快，极具发展潜力。

众多综述文献[32, 59-63]已对分光型、时序调制型、波长调制型等偏振检测技术进行了较为全面的总结，但对空间调制型偏振检测技术的介绍却较少。随着微纳加工与光场调控技术的日益成熟，涡旋波片、角向偏振片、S-波片等空间调制器件被高质量地加工出来，并在偏振检测领域获得了重要的应用。本文首先在研究分析空间调制型偏振检测技术的基础上，对现有空间调制型偏振检测技术及其优缺点进行综述；然后，重点对当前发展非常迅速的基于涡旋波片的空间调制型Stokes及Mueller偏振检测方案进行介绍，详细阐述其工作原理、误差校准方法和潜在应用；最后，对空间调制型偏振检测技术的发展趋势进行展望。

2 空间调制型偏振检测技术发展现状

相较于传统的分光型、时序调制型等偏振检测手段，空间调制型偏振检测技术出现的时间相对较晚，但其光路结构简单、稳定性好、检测性能优异，近年来引起了众多研究人员的关注，发展非常迅速。目前已经发展出基于微偏振片阵列、偏振光栅、双折射楔形棱镜、Savart板、角向或径向偏振片等的偏振检测技术[54-58]。本节主要对这些典型的空间调制型偏振检测技术进行阐述。

2.1 空间调制型Stokes偏振检测技术

2.1.1 分焦平面Stokes偏振仪

分焦平面Stokes偏振仪是空间调制型偏振仪中最常见的一种。如图1(a)所示，其将微偏振片阵列集成在相机的焦平面上，微偏振片阵列的单元尺寸与焦平面像元尺寸需设计一致，焦平面上4个相邻像元组成

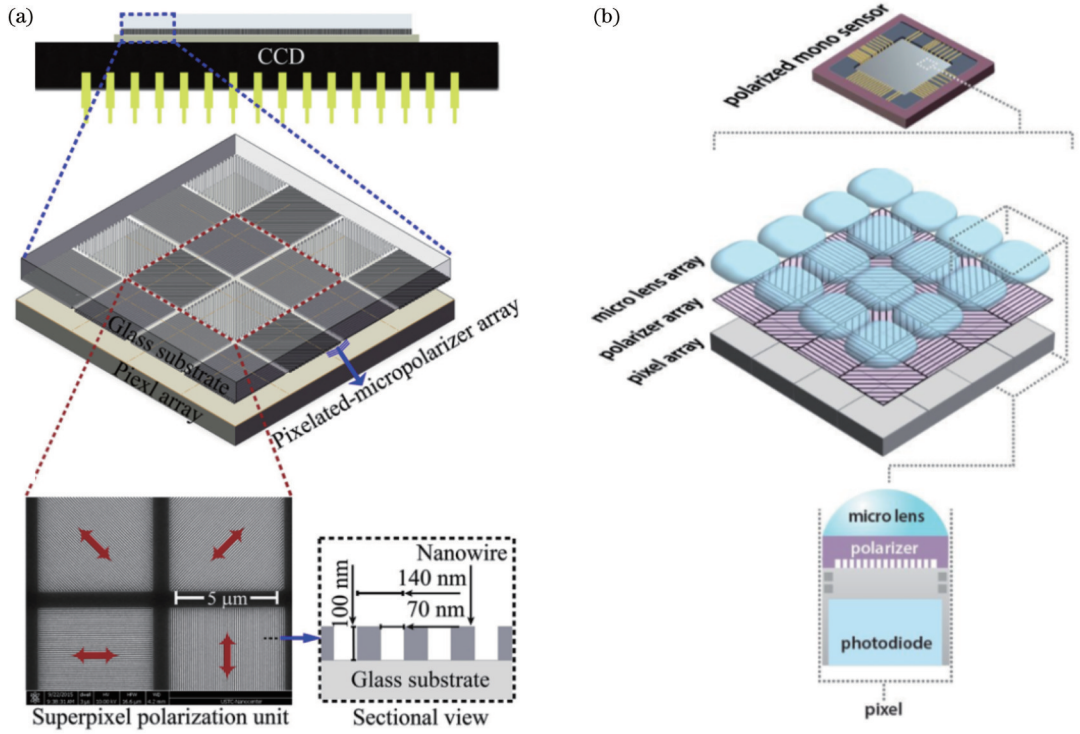

图1 分焦平面Stokes偏振仪。(a)相机传感器结构示意图[64]；(b)IMX250MZR偏振敏感芯片[66]

Fig. 1 Division of focal plane Stokes polarimeter. (a) Schematic of the camera sensor[64]; (b) IMX250MZR polarized mono sensor[66]

一个超像素，这4个像素分别与透光方向不同的微偏振片单元组合，以感应不同方向的偏振矢量，进而实现一个超像素上的偏振检测[64]。分焦平面Stokes偏振仪采用微纳加工元件，结构紧凑，能有效减小设备体积，但微偏振片阵列加工、安装和标定的难度较大[65]。近年来，半导体行业的技术发展使得分焦平面偏振相机的微偏振片阵列可以在光刻阶段实现片上集成，如图1(b)所示，Sony公司研制的IMX250MZR偏振敏感芯片就是将微偏振片阵列集成在探测器与微透镜阵列之间，降低了对准难度，并减小了相邻偏振通道之间的串扰，进一步提升了测量精度[66]。现有的分焦平面偏振相机的微偏振片阵列大多由不同方向的线偏振片组成，其仅能实现线偏振分量的探测，缺乏对圆偏振分量的检测能力，且微偏振片的消光比通常较低、一致性较差。

2.1.2 基于空间偏振片的Stokes偏振仪

不同于普通的偏振片在空间中仅存在一个通光轴方向，偏振光栅、径向或角向偏振片等空间偏振片的通光轴方向在空间中呈现出一定的分布规律，因此可以对光波偏振态产生空间调制效应，并达到与传统时序调制型方法中旋转偏振片相同的效果。

图2(a)为一偏振光栅的结构示意图及其光学显微实拍图，其将亚波长金属条的方向在空间中进行连续变化的周期性排列，振动方向与亚波长金属条方向垂直的光波能够通过，而振动方向与亚波长金属条方向平行的光波将被反射，因此可以将该偏振光栅理解为一个偏振方向在水平方向周期性变化的偏振片，该偏振片的透光轴方向示意图如图2(b)所示。利用该偏振光栅对待测光波的偏振态进行空间调制，得到光强在水平方向连续变化的分布，单次拍图分析即可实现对光波偏振态的检测。但是该方法仅能测量得到待测光波的线偏振分量，而反映圆偏振分量的第4个Stokes参量无法直接测量得到。此外，该偏振光栅的加工难度较大，精度也较低，其对偏振方向的测量精度仅为0.6°[67]。

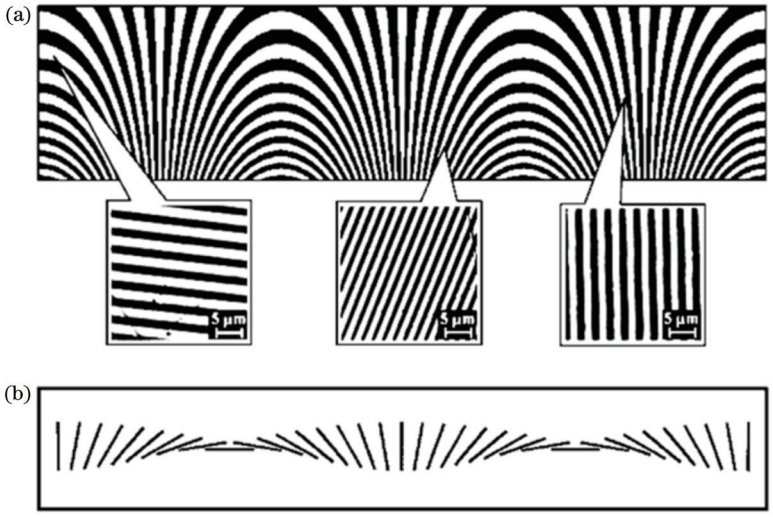

图2 偏振光栅[67]。(a)结构示意及实拍图；(b)透光方向示意图

Fig. 2 Polarization grating[67]. (a) Geometry of the grating and images of the grating taken with an optical microscope; (b) transmission axis of the grating

图3(a)、(b)分别为径向和角向偏振片的通光轴方向分布，一束线偏振光经过径向或角向偏振片调制后会形成一个沿方位角方向亮暗交替分布的“楔形”光强图案，如图3(c)、(d)所示，亮区或暗区中心线方向即为线偏振光的偏振方向。借助其直观成像的特点，国防科技大学Zhang等[27]利用径向偏振片实现了天空散射光的偏振方向与偏振度的测量，并将该方法成功用于仿生偏振导航中，但其获得的测量精度较低、测量速度较慢。太原理工大学Zhang等[68]利用角向偏振片实现了对光波偏振方向的测量，并将其应用于旋光性检测，该方法对偏振方向的测量精度和稳定性分别达到0.143°和0.016°。此外，本课题组也利用角向偏振片实现了对光波偏振方向的测量，并通过设计优化光路结构和图像处理算法将测量精度提升至0.01°[58]。

2.1.3 基于双折射分束器的干涉型Stokes偏振仪

空间调制干涉型Stokes偏振仪采用Savart板、双折射楔形棱镜等双折射分束器，在空间上将待测光波分成多个具有恒定相位差的子光束，如图4中彩色线所示，这些光束经过检偏器后满足稳定干涉条件，经过成像透镜的会聚，在CCD上形成干涉条纹，对采集到的干涉条纹进行解算，即可求解出待测光束的Stokes参量[69]。该方法能够实现偏振态的快速测量，但其缺点是系统组成复杂，且干涉图样的解算过程较为繁琐。

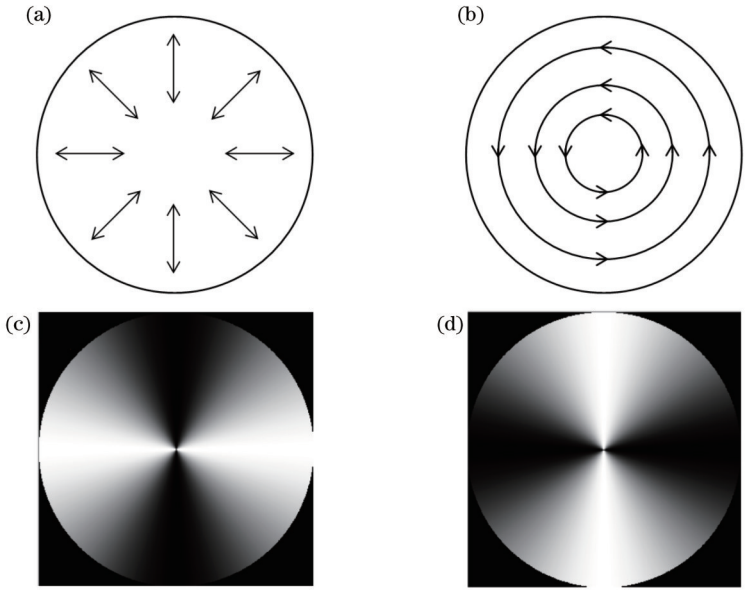

图 3 径向和角向偏振片的通光轴方向分布及水平线偏振光通过后的调制图像。(a)(c)径向偏振片;(b)(d)角向偏振片

Fig. 3 Transmission axis of radial polarizer and azimuthal polarizer and modulated intensity images of horizontal liner polarized light. (a) (c) Radial polarizer; (b) (d) azimuthal polarizer

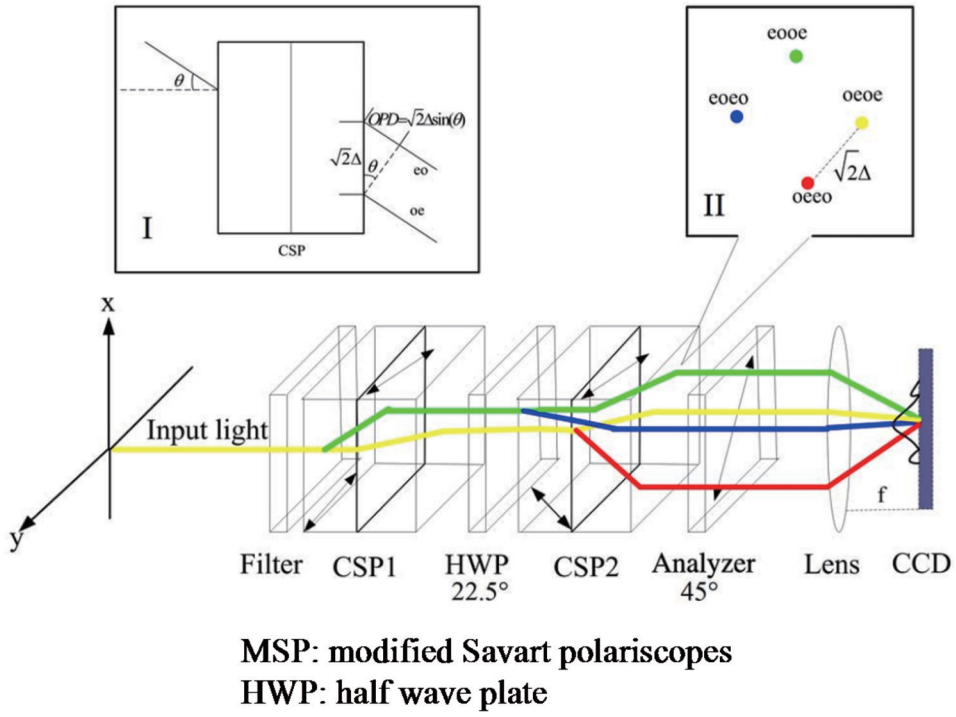

图 4 基于 Savart 板的干涉型 Stokes 偏振仪示意图[69]

Fig. 4 Schematic of the interferometric Stokes polarimeter based on Savart polariscopes[69]

2.2 空间调制型 Mueller 矩阵偏振检测技术

2.2.1 基于矢量光束的 Mueller 矩阵偏振仪

矢量光束是一种结构光场,其在波面上具有空间各异的偏振态分布[70-72],因而在偏振检测方面表现出独特的优势。Tripathi 等[73]采用矢量光束作为入射光,提出一种快速 Mueller 矩阵偏振仪(RAMMP),其装置示意图如图 5(a)所示。矢量光束生成器(VBG)用于产生偏振态空间分布各异的矢量光束[偏振态空间分布如图 5(b)所示],该矢量光束被物镜会聚后通过 1/4 波片并被聚焦至样品表面,经过反射再次通过 1/4 波片并被物镜准直,而后被检偏器检偏后形成空间变化的光强分布,该光强图像被 CCD 相机采集,通过对光强图像进行分析处理即可提取出待测样品的 Mueller 矩阵元素。该 Mueller 矩阵偏振仪的起偏臂采

用空间调制的方法，利用偏振分布空间各异的矢量光束作为入射光束，但是其检偏臂由固定的1/4波片与检偏器组成，无法实现全偏振分析，仅能测量得到12个Mueller矩阵元素。

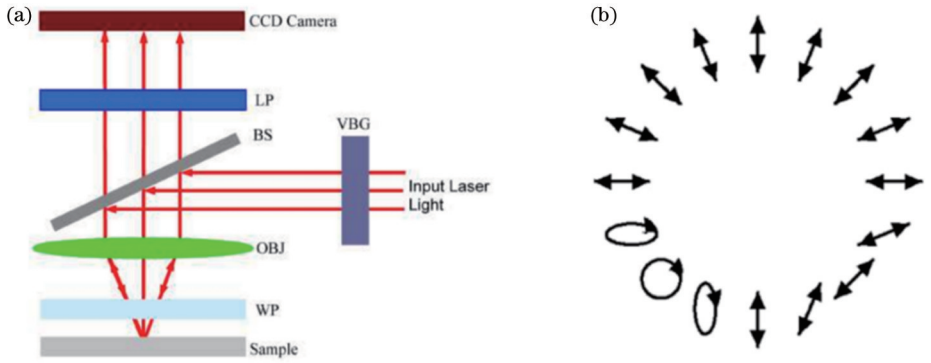

图5 快速Mueller矩阵偏振仪[73]。(a)装置示意图；(b)VBG产生的矢量光束偏振态的空间分布

Fig. 5 Rapid Mueller matrix polarimeter[73]. (a) Schematic of the setup; (b) polarization distribution of vectorial optical field generated by VBG

文献[74-75]分别报道了采用螺旋形矢量光束与角向矢量光束作为入射光进行样品Mueller矩阵检测的方法，但上述两种方法均未实现全Mueller矩阵的测量。为实现全Mueller矩阵测量，Suárez-Bermejo等[76]采用全庞加莱矢量光束作为入射光，全庞加莱光束是一种特殊的矢量偏振光束，庞加莱球表面上任意一点的偏振态均可在全庞加莱光束横截面上找到[71-72]。该方法将全庞加莱光束入射至待测样品，并选取光束横截面上偏振态相互独立的4个点，利用商业Stokes偏振仪对出射光横截面上4个点对应位置处的光波偏振态进行测量，进而计算出待测样品的全部16个Mueller矩阵元素。图6(a)为全庞加莱光束Mueller矩阵偏振仪的结构示意图，图6(b)为其生成的全庞加莱光束的偏振态分布。该Mueller矩阵偏振仪的起偏臂部分采用空间调制的方法，在庞加莱光束横截面上选取4种偏振态相互独立的入射光，但其检偏臂采用商业偏振仪在空间4个位置处分别测量的方法完成偏振态分析，操作过程较为繁琐，且测量速度较慢。

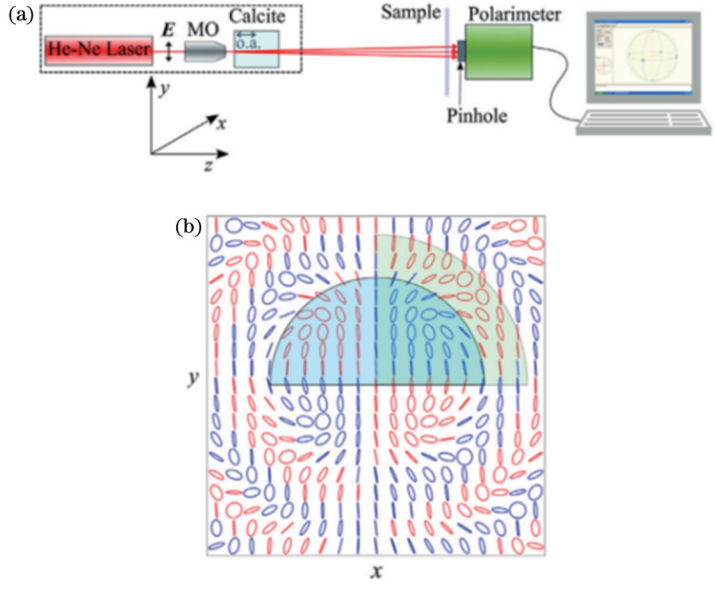

图6 全庞加莱光束Mueller矩阵偏振仪[76]。(a)装置示意图；(b)产生的全庞加莱光束偏振态的空间分布

Fig. 6 Full Poincaré beam Mueller matrix polarimeter[76]. (a) Schematic of the setup; (b) polarization distribution of generated full Poincaré beam

2.2.2 基于轴对称波片的Mueller矩阵偏振仪

基于轴对称波片的Mueller矩阵偏振仪[77]的结构示意图如图7(a)所示，系统中所用的轴对称1/4波片(AQWP)为将30个扇形1/4波片(扇形的圆心角为12°)按照快轴沿一定方向排布拼接而成，AQWP1与AQWP2的快轴方向随方位角的旋转速度之比为1∶5，将它们分别放在两个正交的偏振片中间，观察到的光强图像如图7(b)所示。基于轴对称波片的Mueller矩阵偏振仪在起偏臂和检偏臂分别使用上述两种AQWPs完成对入射光和出射光的空间调制和解调，

单次拍图即可实现待测样品全部Mueller矩阵元素的测量，这为空间调制型Mueller矩阵偏振仪提供了新的思路，但限于AQWP的制作工艺、偏振调制及成像质量等因素，该方案的可行性尚未被实验证明。

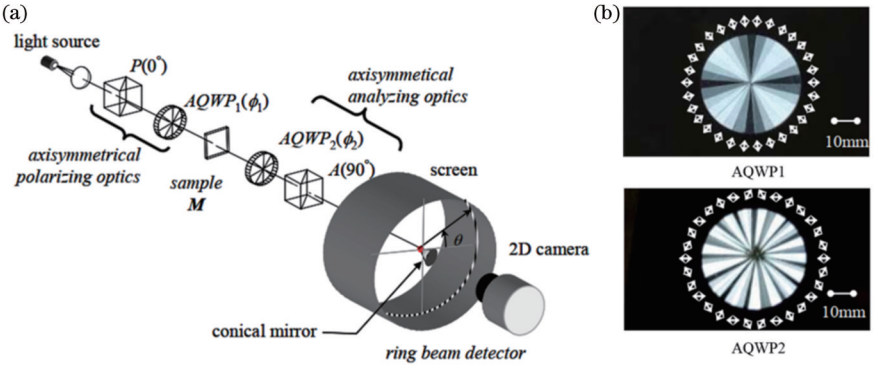

图7 轴对称式Mueller矩阵偏振仪[77]。(a)结构示意图；(b)AQWP在正交偏振片中观察到的光强图像

Fig. 7 Axisymmetrical Mueller matrix polarimeter[77]. (a) Schematic of the setup; (b) AQWPs crossed between polarizers

2.2.3 基于双分焦平面偏振相机的Mueller矩阵偏振仪

基于双分焦平面偏振相机的Mueller矩阵偏振仪[78]的结构示意图及装置如图8所示，其起偏臂采用与传统时序型双旋转相位延迟器Mueller矩阵偏振仪起偏臂相同的配置，但检偏臂部分采用半透半反镜将出射光分为两束，其中一束经固定的相位延迟器后被偏振相机采集，另一束则直接被偏振相机采集，结合两台相机在起偏臂不同配置状态下采集的偏振图像，即可分析计算出待测样品的Mueller矩阵。相较于传统的双旋转相位延迟器Mueller矩阵偏振仪，该方案仅包含一个旋转光学元件，系统稳定性和测量速度均有所提升，但由于其起偏臂采用时序调制型方案，故测量速度仍受到一定限制，且该方案采用了两台偏振相机，导致系统的复杂性和对准难度增加。

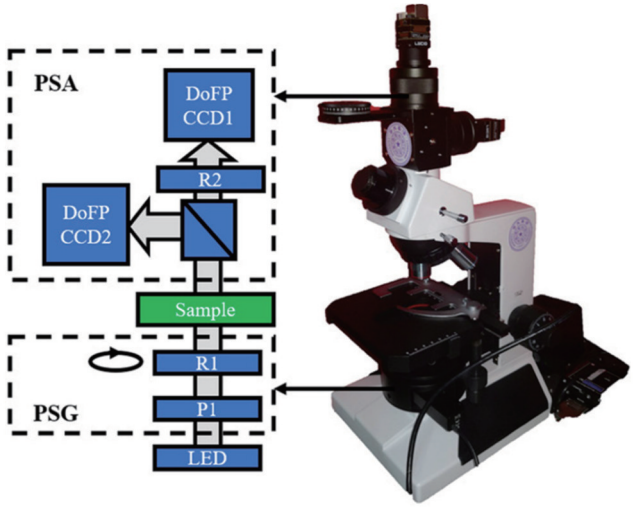

图8 基于双分焦平面偏振相机的Mueller矩阵偏振仪的示意图及实物图[78]

Fig. 8 Schematic and instrument of the dual division of focal plane polarimeters-based Mueller matrix polarimeter[78]

3 基于涡旋波片的空间调制型偏振检测技术

空间调制型偏振仪不涉及机械运动部件或有源器件，系统结构简单、稳定性好、测量速度快，能够有效克服传统偏振检测方法的缺点，极具发展潜力，但现有的空间调制型偏振仪一般存在空间调制型器件制备困难、调制质量较差、解算过程复杂、测量误差大等缺点，特别地，迄今为止还没有发现能够实现全Mueller矩阵测量的空间调制型Mueller矩阵偏振仪[32]。

与微偏振片阵列、S-波片、偏振光栅、角向偏振片等空间调制型器件相比，涡旋波片具有制作工艺成熟、性能稳定、波长敏感性较低、温度稳定性好、调制质量高和成本较低等优势[79-80]，在偏振检测领域展现出巨大的应用潜力。涡旋波片在整个通光孔径上具有恒定的相位延迟，其快轴在光学区域沿角向连续旋转，并对光波偏振态产生空间调制效应，可达到与传统时序调制型方法中旋转波片相同的效果，但可克服其实时性较差以及机械旋转带来的问题[39, 81-85]。因此，将高质量的涡旋波片作为空间调制器件构建偏振检测系统，不仅可开拓矢量光束应用的新领域，而且有望研制出低成本、高性能的新型偏振检测仪。

3.1 基于涡旋半波片的Stokes偏振仪

基于涡旋半波片的Stokes偏振仪[39, 82]的系统结构如图9所示，偏振检测光路由偏振态产生系统(PSG)与偏振态检测系统(PSA)两部分组成，PSG采用起偏器(P)与1/4波片(QWP)组合的方式产生不同偏振态的待测偏振光场，PSA对待测光场的偏振态进行检测。待测光波进入PSA后被一阶涡旋半波片(VHR)转换为矢量偏振光场，该矢量偏振光场经检偏器(A)检偏后形成光强随方位角空间变化的沙漏型调制图像，光强图像被相机采集并输入计算机进行处理分析，即可解算出待测光波的偏振信息。

采用Stokes-Mueller矩阵理论计算得到出射光的

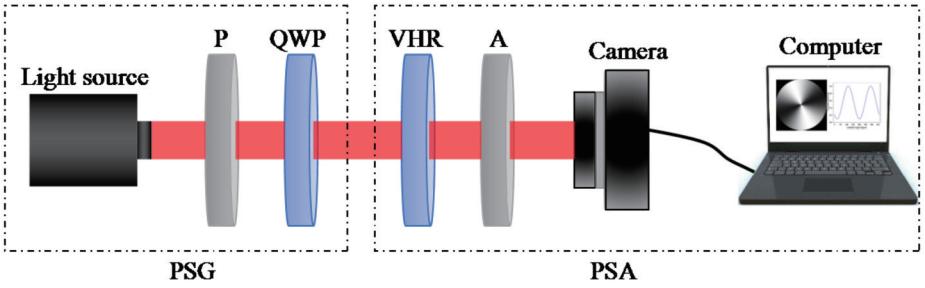

图 9 基于涡旋半波片的 Stokes 偏振仪光路示意图[82]

Fig. 9 Schematic of the vortex half retarder based polarimeter[82]

光强 $I(\varphi)$ 随方位角 φ 的变化规律[39]：

$$I(\varphi)=S_0+S_1\cos(2\varphi)+S_2\sin(2\varphi)。\quad(1)$$

式(1)为截断的傅里叶级数，其傅里叶系数由入射光的 Stokes 参量 $S_i(i=0,1,2)$ 决定。实验中选择光强调制图像成像质量较好的中间圆环部分并沿半径方向进行投影，计算得到各方位角处的光强投影值，并得到光强调制曲线[83]，对光强调制曲线进行傅里叶分析即可得到待测光波的前 3 个 Stokes 参量，而第 4 个 Stokes 参量 S_3 可结合待测光的偏振度和偏振旋向计算得到(图 10)。

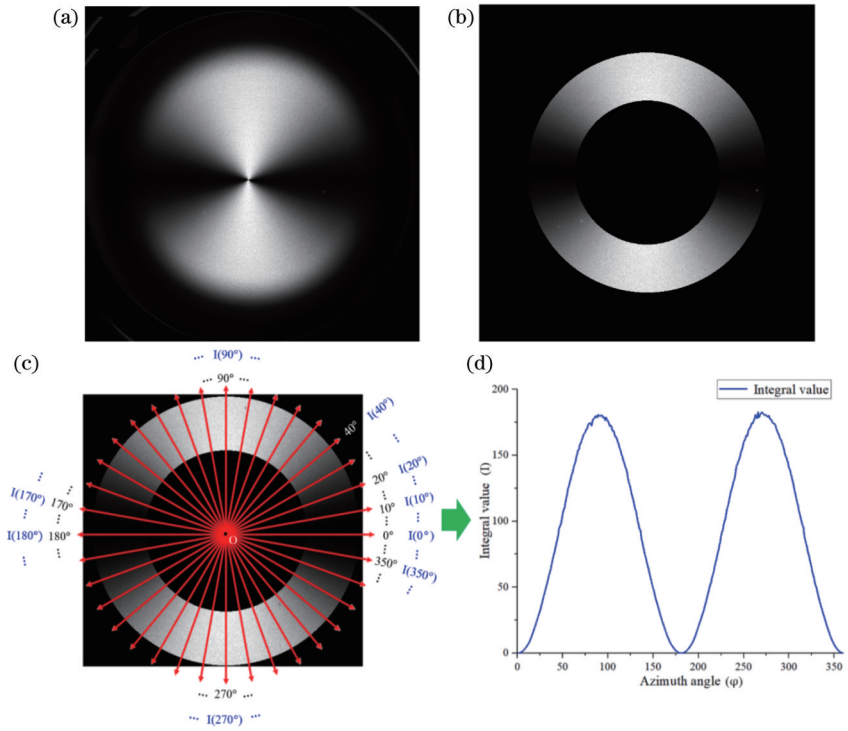

图 10 光强调制曲线获取过程[82]。(a)原始光强图像；(b)截取的调制质量较好的圆环区域；(c)沿各半径方向进行积分；(d)光强调制曲线

Fig. 10 Physical processes to obtain intensity modulated curve[82]. (a) Original intensity image; (b) ring area cut from Fig. 10(a); (c) integrals of ring area along the radius; (d) intensity modulated curve

图 11 展示了该 Stokes 偏振仪对 37 组步进连续变化偏振态进行测量的结果，可以看到，测量结果与理论曲线吻合得较好，进一步计算可知 Stokes 参量 S_1～S_3 的最大测量误差分别为 0.0391、0.0319 与 0.0555；Stokes 参量 S_1～S_3 测量误差的平均值分别为 0.0252、0.0166 与 0.0203，证明了该方法的可行性与精确性。

基于涡旋波片的空间调制型偏振仪具有速度快、结构紧凑、稳定性好等优点。然而，在实际测量中，各光学元器件的方位角误差、波片的相位延迟误差、光源均匀性误差、环境杂散光和图像噪声等因素均会带来测量误差，极大地限制了其潜在的应用范围。为提高该方案的测量精度，文献[82]提出一种有效的误差校准方法。该方法采用 Stokes-Mueller 矩阵理论，研究了各误差因素对光强调制曲线的整体影响，通过分析发现，对于起偏器透光轴和 1/4 波片快轴的夹角设置为 θ_1 和 θ_2 时所产生的偏振光，其光强调制曲线误差 $\Delta I(\varphi,\theta_1,\theta_2)$ 为

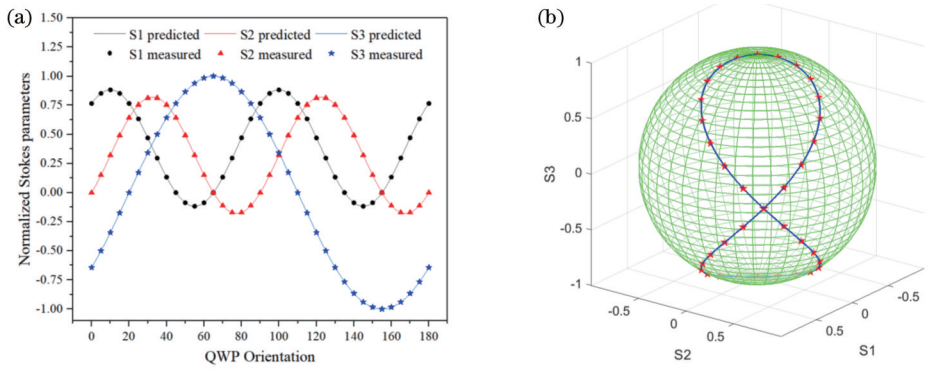

图 11　37 组连续变化偏振态的测量结果[39]。(a)Stokes 参量表示;(b)庞加莱球表述

Fig. 11　Measured results of 37 continuously varying polarization states[39]. (a) Results shown by Stokes parameters; (b) results shown by Poincaré sphere

$$\Delta I(\varphi,\theta_1,\theta_2)=\sin(2\theta_1)\cdot\Delta I(\varphi,45^\circ,\theta_2)+\cos(2\theta_1)\cdot\Delta I(\varphi,0^\circ,\theta_2)+\frac{1}{2}\left[\kappa(\varphi)-1\right]\left[1-\sin(2\theta_1)-\cos(2\theta_1)\right]+N(\varphi)。\tag{2}$$

由式(2)可知:任意偏振态入射光的光强调制曲线误差均可通过 0°和 45°偏振光的光强调制曲线误差 $\Delta I(\varphi,0^\circ,\theta_2)$与 $\Delta I(\varphi,45^\circ,\theta_2)$,并结合光源均匀性误差 $\kappa(\varphi)$及图像噪声误差 $N(\varphi)$叠加计算得到。

为验证该误差校准方法的可行性,采用基于涡旋半波片的 Stokes 偏振仪对 31 组连续变化的偏振态进行测量,各 Stokes 参量的直接测量结果及误差分别如图 12(a)、(c)所示;采用该误差校准方法对上述直接测量结果进行校准后的结果如图 12(b)、(d)所示。通过对比可知,采用该误差校准方法后,Stokes 参量的最大测量误差从 0.0414 下降到 0.0089,测量误差绝对值的平均值由 0.0248 下降到 0.0018,该精度优于市场上一些主流 Stokes 偏振仪的精度[82]。

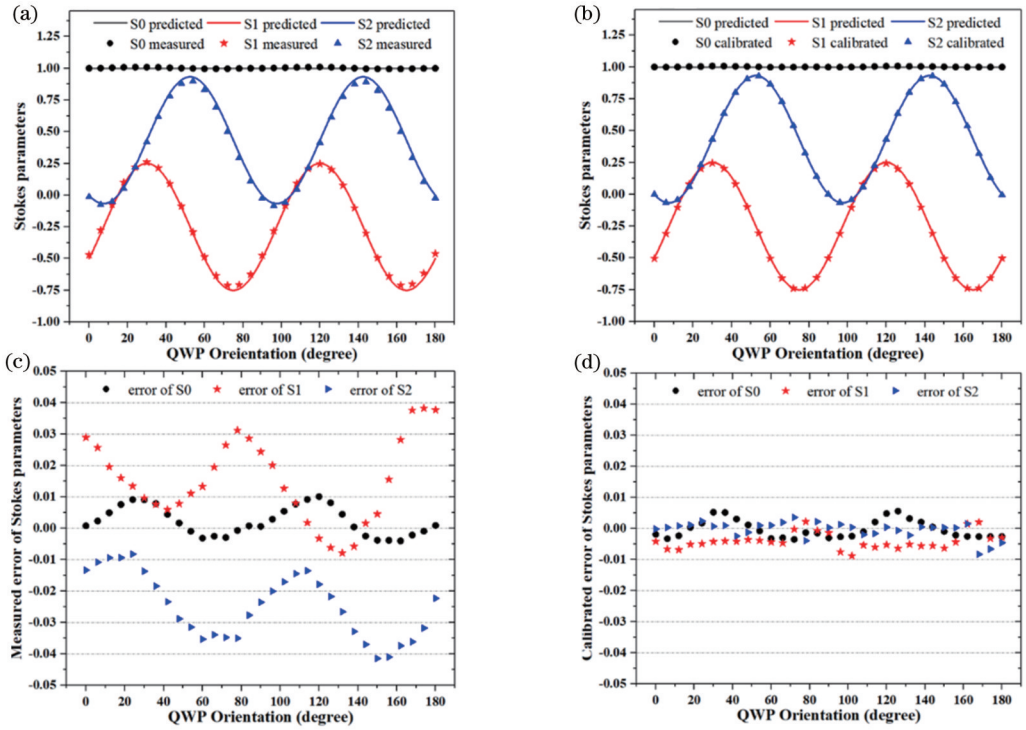

图 12　31 组连续变化偏振态测量及校准结果[82]。(a)直接测量结果;(b)校准后结果;(c)直接测量误差;(d)校准后误差

Fig. 12　Direct measured and calibrated experimental results of 31 different polarization states[82]. (a) Direct measured and (b) calibrated Stokes parameters; (c) direct measured errors and (d) calibrated errors of Stokes parameters

3.2 基于涡旋1/4波片的Stokes偏振仪

基于涡旋半波片的Stokes偏振仪仅能直接测量得到前3个Stokes参量，若待测光波的偏振度或偏振旋向未知，则表示圆偏振信息的第4个Stokes参量将无法计算得到，这就限制了该偏振仪的应用范围。若将系统中的涡旋半波片换成一阶涡旋1/4波片，则出射光的光强[84]为

$$I(\varphi)=S_0+\frac{1}{2}S_1+\frac{1}{2}S_1\cos(2\varphi)+\frac{1}{2}S_2\sin(2\varphi)-S_3\sin\varphi。\tag{3}$$

式(3)相较于式(1)增加了一次谐波项(系数由S_3参量决定)，因而调制规律更为复杂，且光强调制图像一般也不再呈对称的沙漏状分布。该式的傅里叶系数中包含了全部Stokes参量，对出射光的光强调制曲线进行傅里叶分析可得到全部Stokes参量。图13展示了采用基于涡旋1/4波片的偏振检测系统对37组连续变化偏振态的Stokes测量结果。由图13可知，37组连续变化偏振态的测量结果与理论曲线吻合得较好，进一步计算得到Stokes参量S_1～S_3的最大测量误差控制在0.035以内，证明了该技术的可行性与精确性。

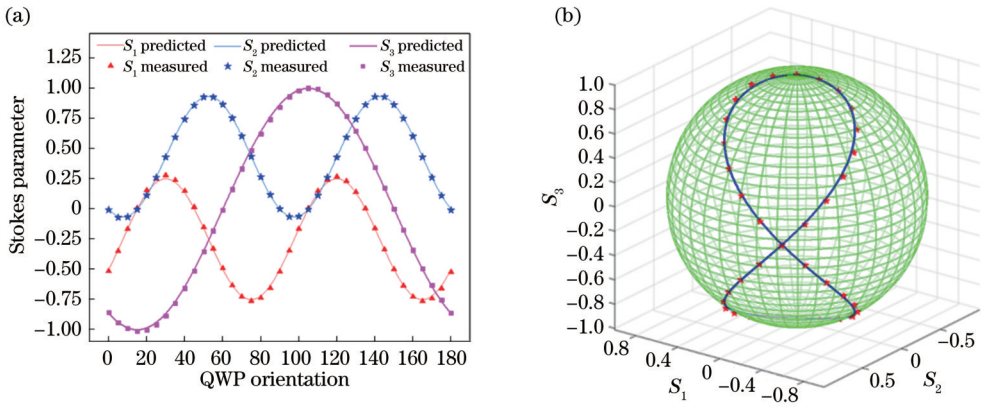

图13 37组连续变化偏振态测量结果。(a)Stokes参量表示；(b)庞加莱球表述

Fig. 13 Measured results of 37 continuously varying polarization states. (a) Results shown by Stokes parameters; (b) results shown by Poincaré sphere

3.3 双涡旋波片Mueller矩阵偏振仪

为实现待测样品全部Mueller矩阵元素的测量，在基于涡旋波片Stokes偏振仪的基础上，提出一种双涡旋波片Mueller矩阵偏振仪[85]。如图14所示，双涡旋波片Mueller矩阵偏振仪由起偏臂和检偏臂两部分组成，其中：起偏臂包含光源、积分球(IS)、准直透镜(L)、起偏器(P)与1阶涡旋1/4波片(V1)；检偏臂包含5阶涡旋1/4波片(V2)、检偏器(A)与相机。光源发出的光经积分球和准直透镜后变为光强空间均匀且近似准直的光束，其经起偏器后变为一束线偏振光，该线偏振光经涡旋波片V1的空间调制后变为偏振态随方位角空间变化的矢量光束，该矢量光束经样品透射或反射之后，其偏振态一般会发生改变，这一变化可由样品的Mueller矩阵表示，透射光束再次经涡旋波片V2空间调制并被检偏器检偏后变为光强随方位角空间变化的出射光，利用相机对光强图案进行采集。

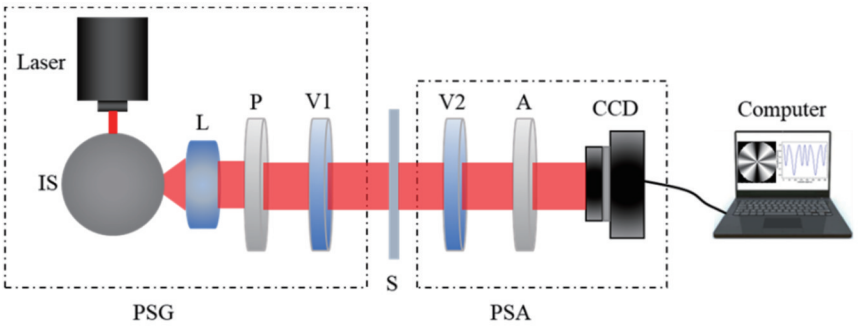

图14 双涡旋波片Mueller矩阵椭偏检测系统装置示意图[85]

Fig. 14 Configuration of dual vortex retarder Mueller matrix polarimeter[85]

采用Stokes-Mueller矩阵理论对出射光的光强$I(\varphi)$随方位角φ的变化规律进行计算并对其进行傅里叶分析，得到

$$I(\varphi)=a_0+\sum_{n=1}^{12}\left[a_n\cos(n\varphi)+b_n\sin(n\varphi)\right]。\tag{4}$$

式(4)中常数项及各谐波级次的傅里叶系数a_0、a_n与b_n($n=1,2,3,\cdots,12$)由待测样品的Mueller矩阵元

素 $m_{ij}(i,j=1,2,3,4)$决定，实验中通过对光强调制图像进行分析处理得到各傅里叶系数，即可反解得到待测样品的全部Mueller矩阵元素。

实验中各光学元器件的方位角误差、波片的相位延迟误差、涡旋波片快轴旋转不均匀误差、环境杂散光和图像噪声等因素均会带来实验误差。为实现对双涡旋波片Mueller矩阵偏振仪的校准，提出一种不依赖于模型的调制矢量校准法，该方法从Mueller矩阵偏振检测系统所要解决的方程$I=\boldsymbol{a}\cdot M_s\cdot\boldsymbol{p}$入手，采用偏振片、1/4波片等标准偏振光学元件对起偏臂与检偏臂的调制矢量$\boldsymbol{p}$与$\boldsymbol{a}$进行测量标定，从而完成对双涡旋波片Mueller矩阵偏振仪起偏臂与检偏臂的校准。

利用双涡旋波片Mueller矩阵偏振仪对空气、不同方位角的偏振片和波片的Mueller矩阵进行测量，各样品的Mueller矩阵调制图像如图15所示。采用调制矢量法校准后得到的Mueller矩阵元测量结果如图16所示，结果表明，测量得到的8种样品Mueller矩阵元素均方根误差和最大误差分别低于0.02和0.04，验证了空间调制型偏振检测系统用于Mueller矩阵测量的可行性。

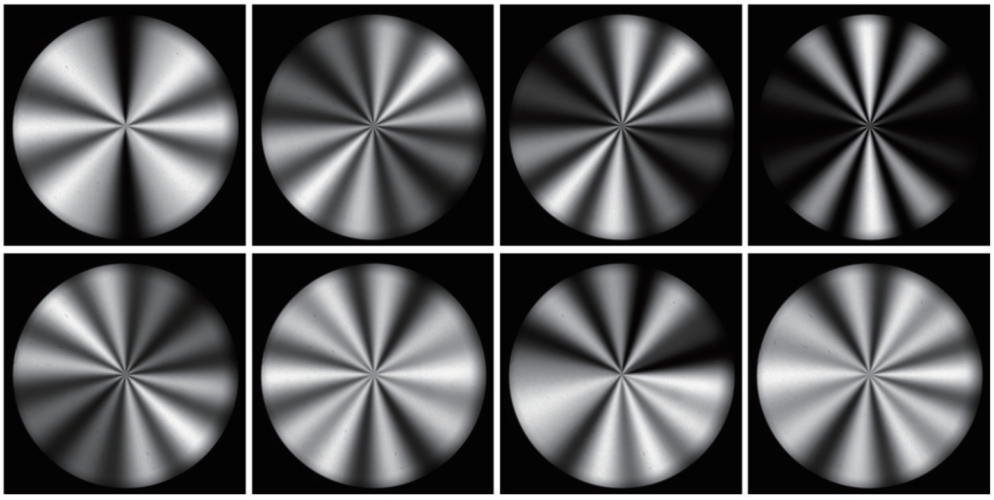

图15　8种样品的光强调制图像[85]

Fig. 15　Captured modulated intensity images of eight samples[85]

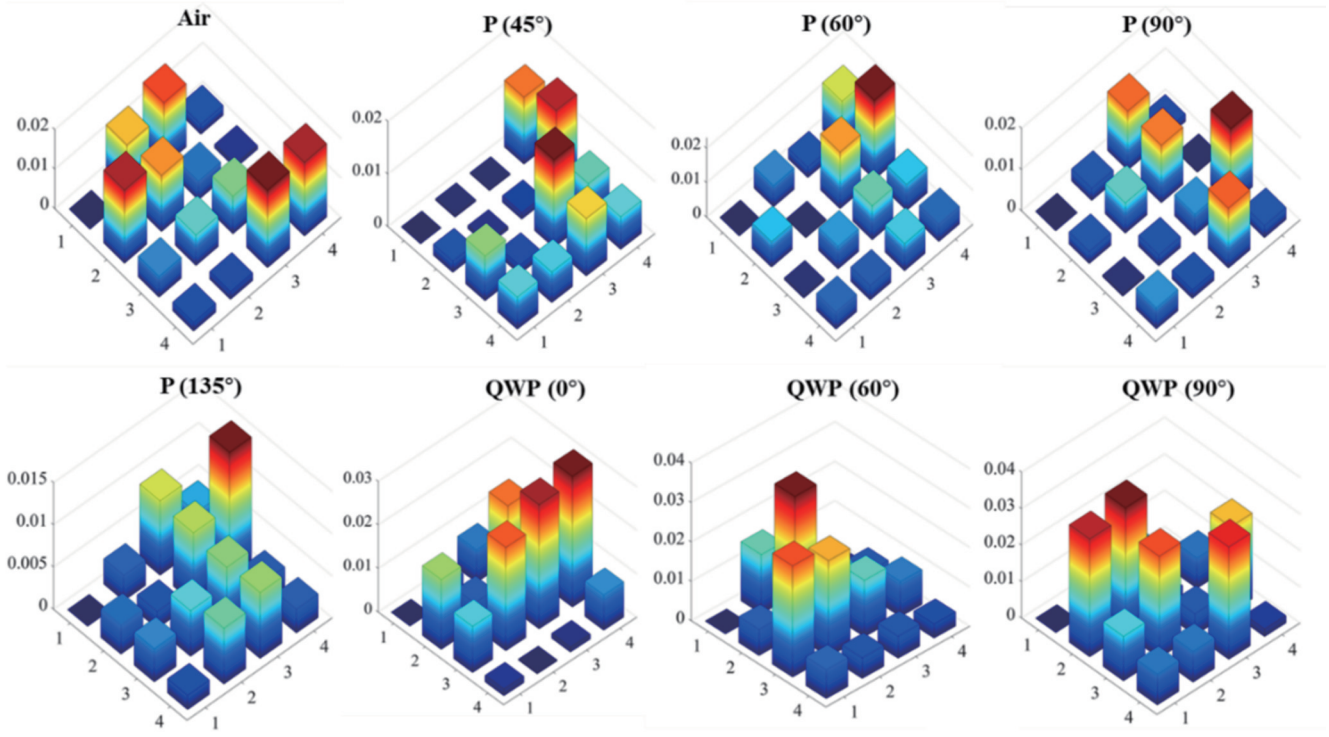

图16　各Mueller矩阵元素测量误差的绝对值[85]

Fig. 16　Absolute values of the measured error for each element in the Mueller matrix[85]

4 空间调制型偏振检测技术发展趋势

近年来，随着材料科学、集成电路等领域的不断发展，相应的生产加工、测试及实时监测等标准也不断提高，这对偏振检测技术的测量精度、速度、空间分辨率，以及小型化和集成化等提出了更为严格的要求。偏振检测技术需要不断地进行研究和发展，同时也需要加强与人工智能、材料科学等相关学科的交叉结合，推动偏振检测技术的创新与应用。

1）与深度学习结合

如何从光强空间分布的调制图像提取出偏振信息是空间调制型偏振检测技术的关键问题之一，其包含光强调制特征的提取和偏振信息解算两个部分。一方面，不同类型的空间调制型器件具有不同的调制规律，所产生光强图像的调制特征也是不同的，传统的做法是结合调制器件的调制规律及调制图像的特征，通过编写相应的图像处理算法来完成光强调制特征的提取。这一过程通常较为直观，但在某些情况下[69]，空间调制型偏振检测系统所产生的光强调制图像较为复杂，相应的图像处理算法也变得复杂，图像处理速度、精度等都会受到一定限制。另一方面，作为一种间接测量方法，偏振检测技术需要根据测量获得偏振信息，从而反演解算出待测样品的光学特性，这一过程通常需要一定的样品先验信息及偏振检测相关的专业知识，这对偏振检测仪器的操作人员提出了较高的技术要求[32]。深度学习是一种机器学习算法，其基本原理是通过非线性网络结构对数据进行学习和建模。与传统的机器学习算法相比，深度学习算法通过深层神经网络对大量原始数据进行分析，自动提取和抽象输入数据的特征，可以实现更加准确的预测和分类，其在图像处理领域拥有巨大的应用潜力。将深度学习应用于光强调制特征的提取和偏振信息解算[86-90]，有望加快图像处理的速度、提升精度，降低偏振检测中对样品先验信息及操作人员的技术要求。

2）与超材料结合

超材料是一种具有亚波长结构的人工设计材料，具有自然材料所不具备的一些特异性质，通过灵活的设计，它能够以极其紧凑的结构实现对光波多种特性，如光强、相位、偏振等的调制，因而在偏振检测领域也表现出巨大的优势[91-95]。例如：通过集成线性偏振片和圆偏振片功能的像素化超表面可以设计实现全Stokes检测的分焦平面偏振相机[96]；利用其结构紧凑的特性可以设计实现小型化的偏振检测仪，甚至有望实现片上的偏振检测[32]。

3）空间分辨率的提升

空间调制型偏振检测仪在空间上对光波的偏振态进行调制，测量结果必然会损失空间分辨率，这限制了其在集成电路检测、生物医学样品检测等分辨率要求较高场合的应用。为了提高空间调制型偏振检测仪的空间分辨率，可以将微光斑透镜等置于待测样品前后[97]，以获取较小的测量光斑，还可以采用高数值孔径的聚焦透镜结合背焦平面结构的光路[98]来进一步提高其空间分辨率，同时也可以结合微偏振调制阵列与微透镜阵列等实现空间调制型偏振检测仪对待测光波或样品的成像测量。

4）复合调制型偏振检测技术

复合调制型偏振检测技术采用分光型、时序调制型、波长调制型和空间调制型中的两种或多种来实现偏振信息的检测，旨在兼具所使用调制方式的优点并弥补不足，从而提高偏振检测仪的性能和应用范围。例如，对待测样品物质结构与化学组成、多层膜结构和纳米结构等的分析需要偏振检测仪具备光谱测量能力，可以采用空间调制与波长调制相结合的方式，拓宽空间调制型偏振检测仪的测试光谱范围，实现待测样品信息在宽谱范围内的快速、稳定测量[99]。

5 结束语

对光的偏振特性的研究为光学技术的发展和应用提供了丰富的自由度，相应的偏振检测技术也一直备受各国研究人员的关注。经过数百年的发展，多种类型偏振检测技术相继出现，使得偏振检测技术的测量速度、精度、获取信息的丰富程度等不断向更高的台阶迈进。本文对现有的分光型、时序调制型、波长调制型等偏振检测技术进行介绍，并着重对空间调制型偏振检测技术的原理、系统结构、优缺点以及未来可能的发展趋势进行梳理和分析。空间调制型偏振检测技术虽然出现时间较晚，但其优势突出，发展潜力大，发展速度快；同时，微纳加工、深度学习等技术的发展也将为空间调制型偏振检测技术注入新的活力。相信研究人员未来对于空间调制型偏振检测技术的创新将促进偏振检测技术进一步发展，将其应用到相关领域，可获得更多有利于人类社会发展的新成果。

参 考 文 献

[1] 刘智颖，贺文俊，付跃刚. 三维光场偏振理论及应用[M]. 北京：科学出版社，2020：2-9.
Liu Z Y, He W J, Fu Y G. Polarization theory for three-dimensional light field and its applications[M]. Beijing: Science Press, 2020: 2-9.

[2] 赵永强，潘泉，程咏梅. 成像偏振光谱遥感及应用[M]. 北京：国防工业出版社，2011：256.
Zhao Y Q, Pan Q, Cheng Y M. Imaging spectropolarimetric remote sensing and application[M]. Beijing: National Defense Industry Press, 2011: 256.

[3] Chen W, Yan L, Chandrasekar V. Optical polarization remote sensing[J]. International Journal of Remote Sensing, 2020, 41(13): 4849-4852.

[4] Ahmed A, Zhao X J, Bermak A. Polarization imaging for remote sensing[C]//2017 IEEE Microwaves, Radar and Remote Sensing Symposium (MRRS), August 29-31, 2017, Kiev, Ukraine. New York: IEEE Press, 2017: 15-18.

[5] Tyo J S, Goldstein D H, Chenault D B, et al. Polarization in remote sensing: introduction[J]. Applied Optics, 2006, 45(22):

5451-5452.

[6] Löper P, Stuckelberger M, Niesen B, et al. Complex refractive index spectra of $CH_3NH_3PbI_3$ perovskite thin films determined by spectroscopic ellipsometry and spectrophotometry[J]. The Journal of Physical Chemistry Letters, 2015, 6(1): 66-71.

[7] McCrackin F L, Passaglia E, Stromberg R R, et al. Measurement of the thickness and refractive index of very thin films and the optical properties of surfaces by ellipsometry[J]. Journal of Research of the National Bureau of Standards A, 1963, 67A(4): 363-377.

[8] Zhang H Y, Yang S P, De Ruyck K, et al. Fluorescence polarization assays for chemical contaminants in food and environmental analyses[J]. TrAC Trends in Analytical Chemistry, 2019, 114: 293-313.

[9] Mi T J, Wang Z H, Eremin S A, et al. Simultaneous determination of multiple (fluoro) quinolone antibiotics in food samples by a one-step fluorescence polarization immunoassay[J]. Journal of Agricultural and Food Chemistry, 2013, 61(39): 9347-9355.

[10] Novikova T, De Martino A, Hatit S B, et al. Application of Mueller polarimetry in conical diffraction for critical dimension measurements in microelectronics[J]. Applied Optics, 2006, 45(16): 3688-3697.

[11] Liu S Y, Du W C, Chen X G, et al. Mueller matrix imaging ellipsometry for nanostructure metrology[J]. Optics Express, 2015, 23(13): 17316-17329.

[12] Li J, Podraza N J, Collins R W. Real time spectroscopic ellipsometry of sputtered CdTe, CdS, and $CdTe_{1-x}S_x$ thin films for photovoltaic applications[J]. Physica Status Solidi A, 2008, 205(4): 901-904.

[13] Levi D H, Teplin C W, Iwaniczko E, et al. Real-time spectroscopic ellipsometry studies of the growth of amorphous and epitaxial silicon for photovoltaic applications[J]. Journal of Vacuum Science & Technology A, 2006, 24(4): 1676-1683.

[14] Yousaf M S, Ahmad I, Khurshid A, et al. Machine assisted classification of chicken, beef and mutton tissues using optical polarimetry and Bagging model[J]. Photodiagnosis and Photodynamic Therapy, 2020, 31: 101779.

[15] Hoekman D H, Vissers M A M. A new polarimetric classification approach evaluated for agricultural crops[J]. IEEE Transactions on Geoscience and Remote Sensing, 2003, 41(12): 2881-2889.

[16] Liu C, Shang J L, Vachon P W, et al. Multiyear crop monitoring using polarimetric RADARSAT-2 data[J]. IEEE Transactions on Geoscience and Remote Sensing, 2012, 51(4): 2227-2240.

[17] Nee T W, Wang H W, Nee S M F, et al. Polarization/depolarization of non-diffusive anisotropic photon-scattering biomedical tissues[J]. Proceedings of SPIE, 2010, 7792: 77920F.

[18] He C, He H H, Chang J T, et al. Polarisation optics for biomedical and clinical applications: a review[J]. Light: Science & Applications, 2021, 10: 194.

[19] Zhao Y Q, Zhang L, Pan Q A. Spectropolarimetric imaging for pathological analysis of skin[J]. Applied Optics, 2009, 48(10): D236-D246.

[20] 许志兵, 吴进锦, 丁路, 等. 基于偏振和明场多模态显微成像技术的乳腺癌智能诊断研究[J]. 中国激光, 2022, 49(24): 2407102.
Xu Z B, Wu J J, Ding L, et al. Research on intelligent diagnosis of breast cancer based on polarization and bright-field multimodal microscopic imaging technology[J]. Chinese Journal of Lasers, 2022, 49(24): 2407102.

[21] Hasekamp O P, Landgraf J. Retrieval of aerosol properties over the ocean from multispectral single-viewing-angle measurements of intensity and polarization: retrieval approach, information content, and sensitivity study[J]. Journal of Geophysical Research: Atmospheres, 2005, 110(D20): D20207.

[22] Stachnik J C, Sheehan A F, Zietlow D W, et al. Determination of new zealand ocean bottom seismometer orientation via rayleigh-wave polarization[J]. Seismological Research Letters, 2012, 83(4): 704-713.

[23] 邓宇, 付强, 张肃, 等. 基于偏振检测技术的海面太阳耀光抑制方法[J]. 激光与光电子学进展, 2021, 58(20): 2001003.
Deng Y, Fu Q, Zhang S, et al. Method of suppressing sea surface solar flare based on polarization detection technology[J]. Laser & Optoelectronics Progress, 2021, 58(20): 2001003.

[24] Wang G Q, Shao L Y, Xiao D R, et al. Stable and highly efficient free-space optical wireless communication system based on polarization modulation and in-fiber diffraction[J]. Journal of Lightwave Technology, 2021, 39(1): 83-90.

[25] Xavier G B, Vilela de Faria G, Temporão G P, et al. Full polarization control for fiber optical quantum communication systems using polarization encoding[J]. Optics Express, 2008, 16(3): 1867-1873.

[26] 董群锋, 陈博. 基于光信号偏振复用的微波光子信道化接收机[J]. 激光与光电子学进展, 2022, 59(21): 2106004.
Dong Q F, Chen B. Microwave photon channelized receiver based on polarization multiplexing of optical signals[J]. Laser & Optoelectronics Progress, 2022, 59(21): 2106004.

[27] Zhang W J, Zhang X Z, Cao Y, et al. Robust sky light polarization detection with an S-wave plate in a light field camera [J]. Applied Optics, 2016, 55(13): 3518-3525.

[28] Millar-Blanchaer M, Moon D S, Graham J R, et al. Polarization gratings for visible and near-infrared astronomy[J]. Proceedings of SPIE, 2014, 9151: 91514I.

[29] Breckinridge J B, Oppenheimer B R. Polarization effects in reflecting coronagraphs for white-light applications in astronomy [J]. The Astrophysical Journal Letters, 2004, 600(2): 1091-1098.

[30] Goldstein D H. Polarized light[M]. New York: CRC Press, 2017: 353-375.

[31] Tompkins H G, Irene E A. Handbook of ellipsometry[M]. New York: William Andrew, 2005: 3-91.

[32] Chen X G, Gu H G, Liu J M, et al. Advanced Mueller matrix ellipsometry: instrumentation and emerging applications[J]. Science China Technological Sciences, 2022, 65(9): 2007-2030.

[33] Perez J J G, Ossikovski R. Polarized light and the Mueller matrix approach[M]. New Taylor & Francis Group, 2016: 167-196.

[34] 贺虎成. 分孔径同时偏振成像光学系统的研究[D]. 苏州: 苏州大学, 2014.
He H C. Study on optical system of simultaneous polarization imaging with sub-aperture[D]. Suzhou: Soochow University, 2014.

[35] Negara C, Li Z, Längle T, et al. Simplified Stokes polarimeter based on division-of-amplitude[J]. Proceedings of SPIE, 2019, 11144: 111441B.

[36] Compain E, Drevillon B. Broadband division-of-amplitude polarimeter based on uncoated prisms[J]. Applied Optics, 1998, 37(25): 5938-5944.

[37] Calixto S, Martinez-Ponce G, Garnica G, et al. A wavefront division polarimeter for the measurements of solute concentrations in solutions[J]. Sensors, 2017, 17(12): 2844.

[38] Laude-Boulesteix B, De Martino A, Drévillon B, et al. Mueller polarimetric imaging system with liquid crystals[J]. Applied Optics, 2004, 43(14): 2824-2832.

[39] Gao C, Lei B. Spatially modulated polarimetry based on a vortex retarder and Fourier analysis[J]. Chinese Optics Letters, 2021, 19(2): 021201.

[40] Hagen N. Calibration and demonstration of a snapshot Mueller matrix spectropolarimeter[J]. Proceedings of SPIE, 2021, 11833: 118330L.

[41] Quan N C, Zhang C M, Mu T K, et al. Spectroscopic Mueller

matrix polarimeter based on spectro-temporal modulation[J]. Optics Express, 2020, 28(25): 37758-37772.
[42] Smith M H. Optimization of a dual-rotating-retarder Mueller matrix polarimeter[J]. Applied Optics, 2002, 41(13): 2488-2493.
[43] Williams P A. Rotating-wave-plate Stokes polarimeter for differential group delay measurements of polarization-mode dispersion[J]. Applied Optics, 1999, 38(31): 6508-6515.
[44] Williams P A, Rose A H, Wang C M. Rotating-polarizer polarimeter for accurate retardance measurement[J]. Applied Optics, 1997, 36(25): 6466-6472.
[45] Wang B B, List J, Rockwell R R. Stokes polarimeter using two photoelastic modulators[J]. Proceedings of SPIE, 2002, 4819: 1-8.
[46] FitzGerald W R, Hore D K. Photoelastic modulator-based broadband mid-infrared stokes polarimeter[J]. Journal of Modern Optics, 2018, 65(1): 75-84.
[47] De Martino A, Kim Y K, Garcia-Caurel E, et al. Optimized Mueller polarimeter with liquid crystals[J]. Optics Letters, 2003, 28(8): 616-618.
[48] Garcia-Caurel E, De Martino A, Drévillon B. Spectroscopic Mueller polarimeter based on liquid crystal devices[J]. Thin Solid Films, 2004, 455/456: 120-123.
[49] Pust N J, Shaw J A. Dual-field imaging polarimeter using liquid crystal variable retarders[J]. Applied Optics, 2006, 45(22): 5470-5478.
[50] Nistor C, Beach G S D, Erskine J L. Versatile magneto-optic Kerr effect polarimeter for studies of domain-wall dynamics in magnetic nanostructures[J]. Review of Scientific Instruments, 2006, 77(10): 103901.
[51] Yasumatsu N, Kasatani A, Oguchi K, et al. High-speed terahertz time-domain polarimeter based on an electro-optic modulation technique[J]. Applied Physics Express, 2014, 7(9): 092401.
[52] Dubreuil M, Rivet S, Le Jeune B, et al. Snapshot Mueller matrix polarimeter by wavelength polarization coding[J]. Optics Express, 2007, 15(21): 13660-13668.
[53] Oka K, Kato T. Spectroscopic polarimetry with a channeled spectrum[J]. Optics Letters, 1999, 24(21): 1475-1477.
[54] Chang J T, Zeng N, He H H, et al. Single-shot spatially modulated Stokes polarimeter based on a GRIN lens[J]. Optics Letters, 2014, 39(9): 2656-2659.
[55] Oka K, Kaneko T. Compact complete imaging polarimeter using birefringent wedge prisms[J]. Optics Express, 2003, 11(13): 1510-1519.
[56] Bo J A, Xing W H, Gu Y T, et al. Spatially modulated snapshot imaging polarimeter using two Savart polariscopes[J]. Applied Optics, 2020, 59(28): 9023-9031.
[57] Davis J A, Moreno I, Holland J E, et al. Multichannel polarization imaging with a polarizing diffraction grating[J]. Optical Engineering, 2017, 56(11): 113104.
[58] Lei B, Liu S G. Efficient polarization direction measurement by utilizing the polarization axis finder and digital image processing [J]. Optics Letters, 2018, 43(12): 2969-2972.
[59] Azzam R M A. Polarization, thin-film optics, ellipsometry, and polarimetry: retrospective[J]. Journal of Vacuum Science & Technology B, 2019, 37(6): 060802.
[60] Azzam R M A. Stokes-vector and Mueller-matrix polarimetry [J]. Journal of the Optical Society of America A, 2016, 33(7): 1396-1408.
[61] Ahmad I, Khaliq A, Iqbal M, et al. Mueller matrix polarimetry for characterization of skin tissue samples: a review[J]. Photodiagnosis and Photodynamic Therapy, 2020, 30: 101708.
[62] Trippe S. Polarization and polarimetry: a review[J]. Journal of the Korean Astronomical Society, 2014, 47(1): 15-39.
[63] 朱绪丹, 张荣君, 郑玉祥, 等. 椭圆偏振光谱测量技术及其在薄膜材料研究中的应用[J]. 中国光学, 2019, 12(6): 1195-1234.
Zhu X D, Zhang R J, Zheng Y X, et al. Spectroscopic ellipsometry and its applications in the study of thin film materials [J]. Chinese Optics, 2019, 12(6): 1195-1234.
[64] Ma X, Dong F L, Zhang Z G, et al. Pixelated-polarization-camera-based polarimetry system for wide real-time optical rotation measurement[J]. Sensors and Actuators B, 2019, 283: 857-864.
[65] 罗海波, 张俊超, 盖兴琴, 等. 偏振成像技术的发展现状与展望[J]. 红外与激光工程, 2022, 51(1): 109-118.
Luo H B, Zhang J C, Gai X Q, et al. Development status and prospects of polarization imaging technology[J]. Infrared and Laser Engineering, 2022, 51(1): 109-118.
[66] LOCIO[EB/OL]. [2023-03-02]. http://thinklucid. cn/tech-briefs/polarization-explained-sony-polarized-sensor/.
[67] Bomzon Z, Biener G, Kleiner V, et al. Spatial Fourier-transform polarimetry using space-variant subwavelength metal-stripe polarizers[J]. Optics Letters. 2001, 26(21): 1711-1713.
[68] Zhang W J, Zhang Z W. Scanning visible polarization-direction-modulation polarimeter for optically active media measurement [J]. Sensors and Actuators B, 2019, 286: 119-124.
[69] Cao Q Z, Zhang C M, DeHoog E. Snapshot imaging polarimeter using modified Savart polariscopes[J]. Applied Optics, 2012, 51(24): 5791-5796.
[70] Han W, Yang Y F, Cheng W, et al. Vectorial optical field generator for the creation of arbitrarily complex fields[J]. Optics Express, 2013, 21(18): 20692-20706.
[71] Zhan Q W. Vectorial optical fields: fundamentals and applications [M]. Singapore: World scientific, 2013: 27-28.
[72] Chen J, Wan C H, Zhan Q W. Vectorial optical fields: recent advances and future prospects[J]. Science Bulletin, 2018, 63(1): 54-74.
[73] Tripathi S, Toussaint K C. Rapid Mueller matrix polarimetry based on parallelized polarization state generation and detection [J]. Optics Express, 2009, 17(24): 21396-21407.
[74] de Sande J C G, Piquero G, Santarsiero M. Polarimetry with azimuthally polarized light[J]. Optics Communications, 2018, 410: 961-965.
[75] de Sande J C G, Santarsiero M, Piquero G. Spirally polarized beams for polarimetry measurements of deterministic and homogeneous samples[J]. Optics and Lasers in Engineering, 2017, 91: 97-105.
[76] Suárez-Bermejo J C, González de Sande J C, Santarsiero M, et al. Mueller matrix polarimetry using full Poincaré beams[J]. Optics and Lasers in Engineering, 2019, 122: 134-141.
[77] Wakayama T, Otani Y, Yoshizawa T. Axisymmetrical Mueller matrix polarimeter[J]. Proceedings of SPIE, 2009, 7461: 74610M.
[78] Huang T Y, Meng R Y, Qi J, et al. Fast Mueller matrix microscope based on dual DoFP polarimeters[J]. Optics Letters, 2021, 46(7): 1676-1679.
[79] THORLABS[EB/OL]. [2023-03-02]. https://www.thorlabschina.cn/newgrouppage9.cfm?objectgroup_id=9098.
[80] Ibtek. com[EB/OL]. [2023-03-02]. https://www. lbtek. com/product/581.html.
[81] Gao C, Lei B. Spatially polarization-modulated ellipsometry based on the vectorial optical field and image processing[J]. Applied Optics, 2020, 59(18): 5377-5384.
[82] Gao C, Wang F J, Wen X K, et al. Error calibration method for a vortex retarder based spatially modulated polarimeter[J]. Measurement, 2023, 212: 112631.
[83] 王富杰, 曹晓昱, 高超, 等. 基于矢量光场空间调制的光波偏振方向解算方法研究[J]. 物理学报, 2023, 72(1): 010201.
Wang F J, Cao X Y, Gao C, et al. Research on the solution method of polarization direction of light wave based on spatial modulation of vector light field[J]. Acta Physica Sinica, 2023, 72(1): 010201.
[84] 高超. 基于空间偏振调制与图像处理的偏振检测技术研究[D]. 长沙: 国防科技大学, 2020.

Gao C. Research on polarization detection technology based on spatial polarization modulation and image processing[D]. Changsha: National University of Defense Technology, 2020.
[85] Gao C, Wang F J, Wen X K, et al. Dual vortex retarder Mueller matrix ellipsometry[J]. Optics and Lasers in Engineering, 2023, 166: 107564.
[86] Weng J Y, Gao C, Lei B. Real-time polarization measurement based on spatially modulated polarimeter and deep learning[J]. Results in Physics, 2023, 46: 106280.
[87] Arunachalam A, Berriel S N, Feit C, et al. Machine learning approach to thickness prediction from *in situ* spectroscopic ellipsometry data for atomic layer deposition processes[J]. Journal of Vacuum Science & Technology A, 2022, 40(1): 012405.
[88] Liu J C, Zhang D, Yu D Q, et al. Machine learning powered ellipsometry[J]. Light: Science & Applications, 2021, 10: 55.
[89] Kim I, Gwak S, Bae Y, et al. Optical spectrum augmentation for machine learning powered spectroscopic ellipsometry[J]. Optics Express, 2022, 30(10): 16909-16920.
[90] Alcaire T, Le Cunff D, Gredy V, et al. Spectroscopic ellipsometry imaging for process deviation detection via machine learning approach[C]//2020 31st Annual SEMI Advanced Semiconductor Manufacturing Conference (ASMC), August 24-26, 2020, Saratoga Springs, NY, USA. New York: IEEE Press, 2020.
[91] Shah Y D, Dada A C, Grant J P, et al. An all-dielectric metasurface polarimeter[J]. ACS Photonics, 2022, 9(10): 3245-3252.
[92] Wang C X, Chen Y R, Meng X Q, et al. Error analysis of a rotating-metasurface polarimeter[J]. Applied Optics, 2022, 61(31): 9163-9167.
[93] Ding F, Chen Y T, Bozhevolnyi S. Metasurface-based polarimeters[J]. Applied Sciences, 2018, 8(4): 594.
[94] Mueller J P B, Leosson K, Capasso F. Ultracompact metasurface in-line polarimeter[J]. Optica, 2016, 3(1): 42-47.
[95] Jiang Q A, Du B W, Jiang M L, et al. Ultrathin circular polarimeter based on chiral plasmonic metasurface and monolayer $MoSe_2$[J]. Nanoscale, 2020, 12(10): 5906-5913.
[96] Zhang C, Hu J P, Dong Y G, et al. High efficiency all-dielectric pixelated metasurface for near-infrared full-Stokes polarization detection[J]. Photonics Research, 2021, 9(4): 583-589.
[97] 李伟奇. 高精度宽光谱Mueller矩阵椭偏仪研制与应用研究[D]. 武汉: 华中科技大学, 2016.
Li W Q. Development and application of high-precision wide-spectrum Muller matrix ellipsometer[D]. Wuhan: Huazhong University of Science and Technology, 2016.
[98] Chen C, Chen X G, Wang C, et al. Imaging Mueller matrix ellipsometry with sub-micron resolution based on back focal plane scanning[J]. Optics Express, 2021, 29(20): 32712-32727.
[99] Oka K, Haga Y J, Michida H. Snapshot Mueller-matrix spectropolarimeter using spectral and spatial carriers[J]. Proceedings of SPIE, 2015, 9613: 96130E.

Research Statues and Prospects of Spatially Modulated Polarimetry

Gao Chao[1,2], Weng Jianyu[1,2], Cao Xiaoyu[1,2], Zhang Bin[1,2], Lei Bing[1,2*]

[1]*College of Advanced Interdisciplinary Studies, National University of Defense Technology, Changsha* 410073, *Hunan, China*;

[2]*Nanhu Laser Laboratory, National University of Defense Technology, Changsha* 410073, *Hunan, China*

Abstract

Significance Polarization is one of the fundamental properties of light waves and an important carrier of information. The technique of measuring polarization is known as polarimetry. Compared with traditional intensity detection methods, polarimetry can significantly enhance the ability to acquire and analyze target information by fully utilizing the polarization characteristics of light waves. Due to its unique advantages, polarimetry has been widely used in various fields such as remote sensing, industrial inspection, biomedical, and environmental monitoring.

The key to polarimetry is to obtain the Stokes vector of the measured light waves or the Mueller matrix of the measured sample, which correspond to the Stokes polarimetry and Mueller matrix polarimetry, respectively. Several methods have been proposed for achieving Stokes polarimetry and Mueller matrix polarimetry, including multi-channel polarimetry, temporally modulated polarimetry, spectral polarization modulated polarimetry, and spatially modulated polarimetry. In the multi-channel method, the incident beam is split into several channels with different polarization optics for analyzing the polarization state. In the last three methods, the incident light is modulated in the time domain, spectral domain, or spatial domain for measuring polarization information. The multi-channel scheme is competent for real-time monitoring, but its configuration is usually complicated to adjust. The configuration of temporally modulated polarimetry is compact, but it is restricted by poor stability and slow measurement speed. The spectral polarization modulated polarimetry obtains polarization information at a single integration interval without rotating or active components, but its measurement accuracy is limited, and its wave band is narrow. In contrast, spatially modulated polarimetry modulates the polarization information at different spatial locations by using the spatial modulation components, and it has the advantage of stability, rapidness, and compactness, so it is a promising technique for polarization measurement.

Numerous review articles have provided comprehensive summaries of multi-channel polarimetry, temporally modulated polarimetry, and spectral polarization modulated polarimetry. However, little attention has been given to

spatially modulated polarimetry. With the increasing maturity of micro-nano fabrication and optical field control technologies, various spatial modulation devices such as vortex retarders, azimuthal polarizers, and S-waveplates have been fabricated with high quality and have gained important applications in the field of polarization detection. Therefore, it is crucial and imperative to consolidate the current research about spatially modulated polarimetry to guide the future development of this field more rationally.

Progress Firstly, the working principles and technical characteristics of various spatially modulated Stokes polarimeters and Mueller matrix polarimeters are analyzed and summarized. In these spatially modulated polarimeters, vector optical beams with spatially inhomogeneous polarization distributions or spatial polarization modulation components such as micro-polarizer arrays, polarization grating, azimuthal or radial polarizers, Savart polariscopes, and handmade axisymmetric quarter-wave plates have been utilized to modulate the spatial distribution of light intensity. This enables the measurement of polarization information in a stable, rapid, and compact way. However, it should be noted that the existing spatially modulated polarimetry is limited by the hard fabrication, poor modulation quality of the spatial polarization modulation components, complex processing procedures, and low accuracy. In particular, there is no configuration yet that can realize accurate Mueller matrix measurement experimentally with the spatial polarization modulation technique.

Secondly, in order to overcome the drawbacks of the traditional spatially modulated polarimeters, vortex retarders with the advantages of mature fabricating processes, good wavelength and temperature stability, high modulation quality, and low cost are utilized to construct the high-performance spatially modulated polarimeter. The vortex half-wave retarder-based Stokes polarimeter (Fig. 9) can achieve polarization measurement in a single shot, and it is fast, stable, and easy to implement. However, the measurement accuracy of the vortex retarder-based Stokes polarimeter is limited by various error sources. In order to reduce the measurement error, an efficient calibration method is proposed by analyzing the general effects of the different error sources on the intensity modulation curve of the incident waves with the Stokes-Mueller formalism. The error calibration method can effectively reduce the measurement error from about 0.05 to less than 0.01 (Fig. 12). The proposed vortex half-wave-based Stokes polarimeter lacks the capability of detecting circular polarization components because the fourth Stokes parameter is calculated indirectly, and the handedness of the input light cannot be recognized. In order to directly measure all the Stokes parameters, a vortex quarter-wave retarder is employed to substitute the vortex half-wave retarder, and experiments show that the measurement accuracy of the vortex quarter-wave retarder-based polarimeter is less than 0.035 (Fig. 13). Based on the vortex retarder-based Stokes polarimeter, a complete dual vortex retarder Mueller matrix polarimetry (Fig. 14) is proposed and experimentally verified by using two vortex quarter wave retarders with different orders in polarization state generation (PSG) arm and polarization state analyzer (PSA) arm, and the maximum absolute error is less than 0.04 (Fig. 16).

Conclusions and Prospects The spatially modulated polarimetry has the advantages of simple optical structure, good stability, fast measurement speed, and high accuracy, and it is promising in target detection and recognition, industrial and biochemical detection, and many other fields. As for the perspective of spatially modulated polarimetry, one direction may be smart polarimetry, which is expected to improve the speed and accuracy of image processing and reduce the prior information of the sample and the technical requirements for operators in polarimetry. In addition, the metasurfaces can be utilized to achieve polarization measurement in a compact size. Furthermore, spatially modulated polarimeters should overcome the limitations in spatial resolution and spectral measurement to expand their application fields.

Key words polarimetry; spatial modulation; Stokes vector; Mueller matrix; vortex retarder